# Nuclear symmetry energy with mesonic cross-couplings in the effective chiral model

Tuhin Malik,[1,*] Kinjal Banerjee,[1,†] T. K. Jha,[1,‡] and B. K. Agrawal[2,3,§]
[1]*Department of Physics, BITS-Pilani, K.K. Birla Goa Campus, Goa 403726, India*
[2]*Saha Institute of Nuclear physics, Kolkata 700064, India*
[3]*Homi Bhabha National Institute, Anushakti Nagar, Mumbai 400094, India*
(Received 27 June 2017; revised manuscript received 1 August 2017; published 6 September 2017)

The effective chiral model is extended by introducing the contributions from the cross-couplings between isovector and isoscalar mesons. These cross-couplings are found to be instrumental in improving the density content of the nuclear symmetry energy. The nuclear symmetry energy as well as its slope and curvature parameters at the saturation density are in harmony with those deduced from a diverse set of experimental data. The equation of state for pure neutron matter at subsaturation densities is also in accordance with the ones obtained from different microscopic models. The maximum mass of a neutron star is consistent with the measurement, and the radius at the canonical mass of the neutron star is within the empirical bounds.

DOI: 10.1103/PhysRevC.96.035803

## I. INTRODUCTION

Over the last decade or so there has been extensive work and debate dedicated to understanding the behavior of nuclear symmetry energy theoretically as well as experimentally, both at low and high densities. This knowledge is helpful in understanding both finite nuclei and nuclear matter aspects such as neutron stars (NSs) and supernovae dynamics, related to the neutron-rich domain. It also helps in understanding the strong forces at the fundamental level at higher densities. Currently available data on nuclear masses and giant dipole polarizability have constrained the values of symmetry energy and its slope parameter to $J \sim 32$ MeV and $L \sim 50-80$ MeV [1–7] at nuclear saturation density ($\rho \sim 0.16$ fm$^{-3}$). However, little is known about their behavior at other densities. Motivated by this, one theoretically tries to modify the basic interactions so as to match with the experimental data wherever available. The different variants of the relativistic mean field (RMF) models could reach out to these values only when the contributions from the cross-coupling of the $\rho$ meson to the $\sigma$ or $\omega$ mesons were included [8–10].

Models based on chiral symmetry were introduced by Gell-Mann and Levy [11]. The importance of chiral symmetry in the study of nuclear matter was emphasized by Lee and Wick [12]. However, the linear chiral sigma models fail to describe properties of finite nuclei. In such models, the normal vacuum jumps to a chirally restored abnormal vacuum (Lee-Wick vacuum) [12,13]. This phenomenon is referred to as the chiral collapse problem [14] and it can be overcome mainly in two ways. One of the approaches is to incorporate logarithmic terms of the scalar field in chiral potentials [15–19] which prevents the normal vacuum from collapsing. This class of chiral models is phenomenologically successful in describing finite nuclei [20–23]. However, these models explicitly break the chiral symmetry and are divergent when chiral symmetry is restored [15].

Alternatively, the chiral collapse problem is prevented by generating the isoscalar-vector meson mass dynamically via spontaneous symmetry breaking (SSB) by coupling the isoscalar-vector mesons with the scalar mesons [24,25]. However, initially the main drawback of all these models was the unrealistic high nuclear incompressibility $K$. Later on, in several attempts, the higher order terms of the scalar meson field [26–28] were introduced to ensure a reasonable $K$ at saturation density. The nonlinear terms in the chiral Lagrangian can provide the three-body forces [29] which might have important roles to play at high densities. The effective chiral model has been used to study nuclear matter aspects such as matter at low density and finite temperature [27], NS structure and composition [30], and nuclear matter saturation properties. As emphasized in Ref. [27], the model parameters are constrained and related to the vacuum expectation value of the scalar field. Since the mass of the isoscalar-vector meson is dynamically generated, there are very few free parameters available to adjust the saturation properties. However, this type of model has a couple of drawbacks. It yields the symmetry energy slope parameter, $L \sim 90$ MeV, which is a little too large. Also, the symmetry energy at 0.1 fm$^{-3}$ baryon density is $\sim$22 MeV, which is lower than the presently estimated value [1,31].

In the present work, we employ the effective chiral model in which chiral symmetry breaks spontaneously. We extend this model by including the cross-couplings of $\sigma$ and $\omega$ mesons with the $\rho$ meson. We would like to see whether these terms in the interaction help in fixing the values of symmetry energy and its slope parameter at the saturation density. We study the effects of the cross-couplings on the equation of state (EOS) for asymmetric nuclear matter (ANM). The effects of the crustal EOS on the mass and radius of a NS are evaluated using the method suggested recently by Zdunik *et al.* [32].

The paper is organized as follows. We briefly describe the model in Sec. II. In Sec. III we construct three different models with no cross-coupling, the $\sigma$-$\rho$ cross-coupling, and the $\omega$-$\rho$ cross-coupling and corresponding results are discussed. Conclusions are drawn in Sec. IV.

*tuhin.malik@gmail.com
†kinjalb@goa.bits-pilani.ac.in
‡tkjha@goa.bits-pilani.ac.in
§bijay.agrawal@saha.ac.in

 

## II. MODEL

The complete Lagrangian density for the effective chiral model which includes the various cross-coupling terms is given by

$$\mathcal{L} = \mathcal{L}_l + \mathcal{L}_\times, \tag{1}$$

where

$$\begin{aligned}\mathcal{L}_l = \bar{\psi}_B\Big[\Big(i\gamma_\mu\partial^\mu - g_\omega\gamma_\mu\omega^\mu - \frac{1}{2}g_\rho\vec{\rho}_\mu\cdot\vec{\tau}\gamma^\mu\Big) \\ - g_\sigma(\sigma + i\gamma_5\vec{\tau}\cdot\vec{\pi})\Big]\psi_B + \frac{1}{2}(\partial_\mu\vec{\pi}\cdot\partial^\mu\vec{\pi} + \partial_\mu\sigma\partial^\mu\sigma) \\ - \frac{\lambda}{4}\big(x^2 - x_0^2\big)^2 - \frac{\lambda b}{6m^2}\big(x^2 - x_0^2\big)^3 \\ - \frac{\lambda c}{8m^4}\big(x^2 - x_0^2\big)^4 - \frac{1}{4}F_{\mu\nu}F^{\mu\nu} + \frac{1}{2}g_\omega^2x^2(\omega_\mu\omega^\mu) \\ - \frac{1}{4}\vec{R}_{\mu\nu}\cdot\vec{R}^{\mu\nu} + \frac{1}{2}m_\rho'^{\,2}\vec{\rho}_\mu\cdot\vec{\rho}^\mu,\end{aligned} \tag{2}$$

and

$$\mathcal{L}_\times = \eta_1\Big(\frac{1}{2}g_\rho^2x^2\vec{\rho}_\mu\cdot\vec{\rho}^\mu\Big) + \eta_2\Big(\frac{1}{2}g_\rho^2\vec{\rho}_\mu\cdot\vec{\rho}^\mu\omega_\mu\omega^\mu\Big). \tag{3}$$

Here $\psi_B$ is the nucleon isospin doublet interacting with different mesons $\sigma$, $\omega$, and $\rho$, with the respective coupling strengths $g_i$, with $i = \sigma,\omega$, and $\rho$. The $b$ and $c$ are the strengths for self-couplings of scalar fields. The $\gamma^\mu$ are the Dirac matrices and $\tau$ are the Pauli matrices. $\mathcal{L}_l$ [Eq. (2)] is the original Lagrangian given in Ref. [30]. Note that the potentials for the scalar fields ($\pi$,$\sigma$) are written in terms of a chiral invariant field $x$ given by $x^2 = \pi^2 + \sigma^2$.

In Eq. (3), $\mathcal{L}_\times$ is the new additional piece we add to the original Lagrangian given in [30]. It contains cross-coupling terms between $\rho$ and $\omega$ and also between $\rho$ and $\sigma$. The coupling strength for $\sigma$-$\rho$ and $\omega$-$\rho$ are given by $\eta_1 g_\rho^2$ and $\eta_2 g_\rho^2$ respectively. The interaction of the scalar ($\sigma$) and the pseudoscalar ($\pi$) mesons with the isoscalar-vector meson ($\omega$) generates a dynamical mass for the $\omega$ meson through SSB of the chiral symmetry with scalar field attaining the vacuum expectation value $x_0$. Then the masses of the nucleon ($m$) and the scalar ($m_\sigma$) and vector ($m_\omega$) mesons are related to $x_0$ (vacuum expectation of $x$) through

$$m = g_\sigma x_0, \quad m_\sigma = \sqrt{2\lambda}x_0, \quad m_\omega = g_\omega x_0, \tag{4}$$

where $\lambda = \frac{(m_\sigma^2 - m_\pi^2)}{2f_\pi^2}$ and $f_\pi = x_0$ is the pion decay constant, which reflects the strength of SSB. In Eq. (3) when $\eta_1 \neq 0$ there is a cross-interaction between $\rho$ and $\sigma$. Hence a fraction of the $\rho$ meson mass will come from SSB. The mass of the $\rho$ meson ($m_\rho$) in this model then will be related to the vacuum expectation of $x$ through

$$m_\rho^2 = m_\rho'^{\,2} + \eta_1 g_\rho^2 x_0^2. \tag{5}$$

In the mean field treatment the explicit role of the pion mass is ignored and hence $m_\pi = 0$ and the mesonic field is assumed to be uniform, i.e., without any quantum fluctuation. Then, the isoscalar-vector field $\omega$ is of the form $\omega_\mu = \omega_0\delta_\mu^0$, where $\delta_\mu^0$ is the Kronecker delta. Note that $\omega_0$ does not depend on space-time but it depends on baryon density ($\rho$). The vector field ($\omega$), scalar field ($\sigma$), and isovector field ($\rho_3^0$) equations (in terms of $Y = x/x_0 = m^*/m$) are, respectively, given by

$$\big[m_\omega^2Y^2 + \eta_2C_\rho m_\rho^2\big(\rho_3^0\big)^2\big]\omega_0 = g_\omega\rho, \tag{6}$$

$$\begin{aligned}(1 - Y^2) - \frac{b}{m^2C_\omega}(1 - Y^2)^2 + \frac{c}{m^4C_\omega^2}(1 - Y^2)^3 \\ + \frac{2C_\sigma m_\omega^2\omega_0^2}{m^2} + \frac{2\eta_1C_\sigma C_\rho m_\rho^2\big(\rho_3^0\big)^2}{C_\omega m^2} - \frac{2C_\sigma\rho_s}{mY} = 0,\end{aligned} \tag{7}$$

$$\begin{aligned}m_\rho^2\big[1 - \eta_1(1 - Y^2)C_\rho/C_\omega + \eta_2C_\rho\omega_0^2\big]\rho_3^0 \\ = \frac{1}{2}g_\rho(\rho_p - \rho_n).\end{aligned} \tag{8}$$

The quantities $\rho$ and $\rho_S$ are the baryon and scalar densities defined as

$$\rho = \frac{\gamma}{(2\pi)^3}\int_0^{k_F} d^3k, \tag{9}$$

$$\rho_s = \frac{\gamma}{(2\pi)^3}\int_0^{k_F}\frac{m^*}{\sqrt{m^{*2} + k^2}}d^3k, \tag{10}$$

where $k_F$ is the baryon fermi momentum and $\gamma$ [for example, $\gamma = 4$ for symmetric nuclear matter (SNM)] is the spin degeneracy factor. $C_\sigma \equiv g_\sigma^2/m_\sigma^2$, $C_\omega \equiv g_\omega^2/m_\omega^2$, and $C_\rho \equiv g_\rho^2/m_\rho^2$ are the scalar, vector, and isovector coupling parameters. The energy density ($\epsilon$) and pressure ($p$) for a given baryon density (in terms of $Y = m^*/m$) in this model are obtained from the stress-energy tensor, and are given as

$$\begin{aligned}\epsilon = \frac{1}{\pi^2}\sum_{k_n,k_p}\int_0^{k_F}k^2\sqrt{k^2 + m^{*2}}dk + \frac{m^2}{8C_\sigma}(1 - Y^2)^2 \\ - \frac{b}{12C_\sigma C_\omega}(1 - Y^2)^3 + \frac{c}{16m^2C_\sigma C_\omega^2}(1 - Y^2)^4 \\ + \frac{1}{2}m_\omega^2\omega_0^2Y^2 + \frac{1}{2}m_\rho^2\big[1 - \eta_1(1 - Y^2)(C_\rho/C_\omega) \\ + 3\eta_2C_\rho\omega_0^2\big]\big(\rho_3^0\big)^2,\end{aligned} \tag{11}$$

$$\begin{aligned}p = \frac{1}{3\pi^2}\sum_{k_n,k_p}\int_0^{k_F}\frac{k^4}{\sqrt{k^2 + m^{*2}}}dk - \frac{m^2}{8C_\sigma}(1 - Y^2)^2 \\ + \frac{b}{12C_\sigma C_\omega}(1 - Y^2)^3 - \frac{c}{16m^2C_\sigma C_\omega^2}(1 - Y^2)^4 \\ + \frac{1}{2}m_\omega^2\omega_0^2Y^2 + \frac{1}{2}m_\rho^2\big[1 - \eta_1(1 - Y^2)(C_\rho/C_\omega) \\ + \eta_2C_\rho\omega_0^2\big]\big(\rho_3^0\big)^2.\end{aligned} \tag{12}$$

For SNM we have to set $k_n = k_p$ and $\rho_3^0 = 0$. As our present knowledge of nuclear matter is mainly confined to normal nuclear matter density ($\rho_0$), coupling constants $C_\sigma \equiv g_\sigma^2/m_\sigma^2$ and $C_\omega \equiv g_\omega^2/m_\omega^2$ are not free parameters in Eqs. (11) and (12). To obtain $C_\sigma$ and $C_\omega$, we solve the field equations (6)–(8) self-consistently while satisfying the nuclear saturation properties. Note that for different values of $Y = x_0/x = m^*/m$, we get different values of $C_\sigma$ and $C_\omega$.

After inclusion of cross-interactions $\mathcal{L}_\times$ [Eq. (3)] the modified symmetry energy $S(\rho)$ in this model is

$$S(\rho) = \frac{k_F^2}{6\sqrt{k_F^2+m^{*2}}} + \frac{C_\rho k_F^3}{12\pi^2(m_\rho^*/m_\rho)^2} + \frac{\eta_2 C_\rho^2 \omega_0^2 k_F^3}{6\pi^2(m_\rho^*/m_\rho)^4} - \frac{2\eta_2 C_\rho^2 C_\omega k_F^9}{27\pi^6 m_\omega^2 Y^4 (m_\rho^*/m_\rho)^4}, \quad (13)$$

where $m_\rho^{*2} = m_\rho^2[1-\eta_1(1-Y^2)(C_\rho/C_\omega)+\eta_2 C_\rho \omega_0^2]$ and $k_F = (3\pi^2\rho/2)^{1/3}$. The coupling parameters $C_\rho$, $\eta_1$, and $\eta_2$ can be evaluated numerically by fixing the symmetry energy $S(\rho)$ and its slope parameter $L$ at saturation density ($\rho_0$). Without cross-couplings ($\eta_1 = \eta_2 = 0$) we revert back to the Lagrangian given in [30].

The symmetry energy can be expanded in a Taylor series around the saturation density ($\rho_0$) as [33]

$$S(\rho) = J_0 + L\epsilon_1 + \frac{1}{2}K_{\rm sym}\epsilon_1^2 + \frac{1}{6}Q_{\rm sym}\epsilon_1^3 + O(\epsilon_1^4), \quad (14)$$

where $\epsilon_1 = \frac{\rho-\rho_0}{3\rho}$. The symmetry energy coefficient at $\rho_0$ is $J_0$ and the other coefficients are defined at $\rho_0$ as [34]

$$L = 3\rho \frac{\partial S(\rho)}{\partial \rho}\Big|_{\rho=\rho_0}, \quad (15)$$

$$K_{\rm sym} = 9\rho^2 \frac{\partial^2 S(\rho)}{\partial \rho^2}\Big|_{\rho=\rho_0}, \quad (16)$$

$$Q_{\rm sym} = 27\rho^3 \frac{\partial^3 S(\rho)}{\partial \rho^3}\Big|_{\rho=\rho_0}. \quad (17)$$

Similarly, the nuclear incompressibility ($K$) of ANM can also be expanded in terms of $\delta$ at $\rho_0$ as $K(\delta) = K + K_\tau\delta^2 + O(\delta^4)$, where $\delta = \frac{(\rho_n-\rho_p)}{\rho}$ is the isospin asymmetry and $K_\tau$ is given by [35]

$$K_\tau = K_{\rm sym} - 6L - \frac{Q_0 L}{K}, \quad (18)$$

where $Q_0 = 27\rho^3 \frac{\delta^3(\epsilon/\rho)}{\delta\rho^3}|_{\rho_0}$ in SNM.

## III. RESULTS AND DISCUSSION

As can be seen from the preceding section, the EOSs of SNM are determined by the coupling parameters $C_\sigma$, $C_\omega$, $b$, and $c$ [Eqs. (11) and (12)]. The values of these coupling parameters and resulting SNM properties at the saturation density are listed in Table I. The values of the model parameters lie in the stable region [36].

The density dependence of symmetry energy $S(\rho)$ is obtained by using three different variants of the present model. We consider the case of no cross-coupling (NCC), the $\sigma$-$\rho$ cross-coupling (SR), and the $\omega$-$\rho$ cross-coupling (WR). Since the NCC model has only one free parameter (i.e., $C_\rho$) there is not enough freedom to vary $J_0$ and $L$ independently. However, the SR and WR models can provide some flexibility to adjust them. Note that in comparison to the earlier models (i.e., NCC type), the inclusion of cross-couplings have important implications on $S(\rho)$. The effects of the cross-couplings grow stronger at high densities which are relevant for the study of NS properties.

TABLE I. Model parameters determined from the properties of SNM such as energy per nucleon $E_0 = -16$ MeV, nuclear incompressibility $K = 247$ MeV, and the nucleon effective mass $Y = m^*/m = 0.864$ at the saturation density $\rho_0 = 0.153$ fm$^{-3}$. The scalar and vector meson coupling parameters are $C_\sigma = g_\sigma^2/m_\sigma^2$ and $C_\omega = g_\omega^2/m_\omega^2$ respectively. $B = b/m^2$ and $C = c/m^4$ are the parameters for the higher order self-couplings of the scalar field with $m$ being the nucleon mass. The nucleon, $\omega$ meson, and $\sigma$ meson masses are 939, 783, and 469 MeV, respectively.

| $C_\sigma$ (fm$^2$) | $C_\omega$ (fm$^2$) | $B$ (fm$^2$) | $C$ (fm$^4$) |
|---|---|---|---|
| 7.057 | 1.757 | −5.796 | 0.001 |

In Table II we list the values of coupling constants ($C_\rho$, $\eta_1$, and $\eta_2$) and the resulting nuclear matter properties: $J_0$, $L$, $K_{\rm sym}$, $Q_{\rm sym}$, and $K_\tau$ at the saturation density $\rho_0$ and $J_1$, the symmetry energy at $\rho_1 = 0.1$ fm$^{-3}$. For the NCC, $C_\rho$ is adjusted to yield $J_0 = 32.5$ MeV. For the SR (WR) model, the value of $C_\rho$ and $\eta_1$ ($\eta_2$) are adjusted to yield $J_0 = 32.5$ MeV and $L = 65$ MeV. These values are compatible with $J_0 = 31.6 \pm 2.66$ MeV and $L = 58.9 \pm 16$ MeV obtained by analyzing various terrestrial experimental information and astrophysical observations [37]. It may be noted that the value of $J_1$ obtained for the NCC model shows a significant deviation from $24.1 \pm 0.8$ MeV [1] and $23.6 \pm 0.3$ MeV [31] obtained by analyzing the experimental data on isovector giant resonances, whereas $J_1$ is in good agreement in the SR and WR models. The value of $L$ obtained with the NCC model is also a little too large. By inclusion of cross-couplings (SR and WR models) the value of $L$ is reduced by $\sim 25\%$ keeping $J_0$ fixed.

In what follows, we shall present our results for the density dependence of symmetry energy, EOSs for the SNM and PNM, and the NS properties obtained using the NCC, SR and WR models. We shall also compare our EOSs and the density dependence of symmetry energy with those calculated for a few selected RMF models, namely, NL3 [38], IUFSU [39], BSP [10], and BKA22 [9]. The NL3 model does not include

TABLE II. Coupling constants $C_\rho$, $\eta_1$, and $\eta_2$ determined from various symmetry energy elements. The mass of the $\rho$ meson is 770 MeV. The values of $C_\rho$ are in units of fm$^2$; $\eta_1$ and $\eta_2$ are dimensionless. All symmetry energy elements are in units of MeV.

| | | NCC | SR | WR |
|---|---|---|---|---|
| Parameters | $C_\rho$ | 5.14 | 12.28 | 6.08 |
| | $\eta_1$ | 0 | −0.79 | 0 |
| | $\eta_2$ | 0 | 0 | 6.49 |
| Nuclear matter | $J_0$ | 32.5 | 32.5 | 32.5 |
| | $J_1$ | 22.30 | 24.49 | 23.68 |
| | $L$ | 87 | 65 | 65 |
| | $K_{\rm sym}$ | −20.09 | −59.16 | −204.78 |
| | $Q_{\rm sym}$ | 58.73 | 356.11 | −88.04 |
| | $K_\tau$ | −434 | −368 | −513 |

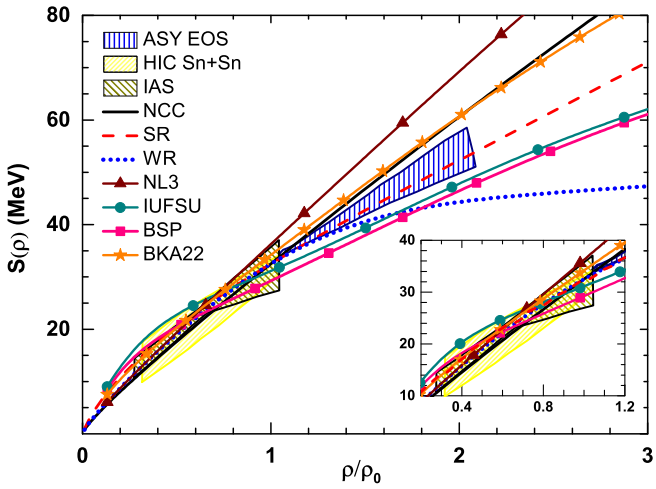


FIG. 1. Symmetry energy as a function of scaled density ($\rho/\rho_0$) is plotted for three different variants of the effective chiral model as labeled by NCC, SR, and WR obtained in the present work and are compared with those for a few selected RMF models: NL3, IUFSU, BSP, and BKA22. The constraints on the symmetry energy from HIC Sn+Sn [40], IAS [41], and ASY-EOS experimental data [42] are also displayed. The inset shows the blown-up behavior of symmetry energy at low densities.

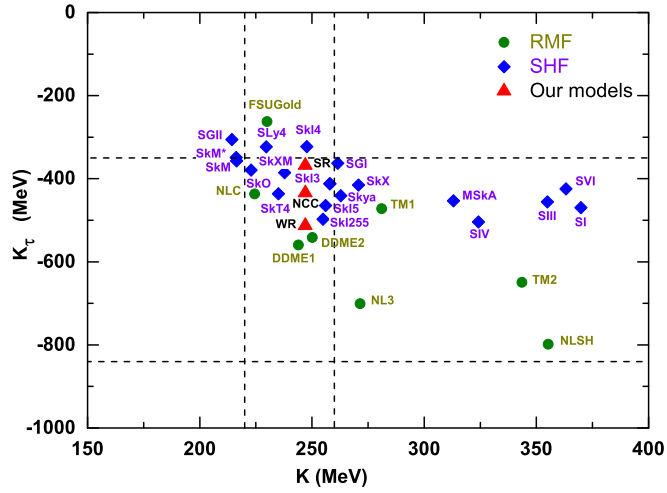


FIG. 2. $K$ and $K_\tau$ from different models as labeled in [43,48] are compared with our models (NCC, SR, and WR). The vertical and horizontal dashed lines represent the empirical ranges for $K$ and $K_\tau$ respectively.

any cross-coupling, the IUFSU and BSP models include the cross-coupling between $\omega$ and $\rho$ mesons, while the BKA22 model is obtained by including the coupling of $\rho$ mesons with $\sigma$ mesons.

A lot of progress, both theoretical and experimental, has been made to constrain symmetry energy at subsaturation densities. We consider the data from three important sources: simulations of low-energy heavy ion collisions (HICs) in $^{112}$Sn and $^{124}$Sn [40]; nuclear structure studies involving excitation energies to isobaric analog states (IASs) [41], and ASY-EOS experiments at GSI [42]. The density dependences of the symmetry energy for NCC, SR, WR, and selected RMF models are displayed in Fig. 1. For comparison we have depicted the HIC Sn+Sn [40], IAS [41], and ASY-EOS [42] data in the figure. It is evident that in the absence of any cross-couplings (NCC), the behavior of symmetry energy as a function of density is not very compatible with those obtained by analyzing diverse experimental data. Remarkably the SR model satisfies all the above-mentioned constraints. None of the considered RMF models satisfy all the symmetry energy constraints. The effects of various cross-couplings on the symmetry energy grow stronger at $\rho > \rho_0$. The symmetry energy is effectively low in the WR model compared to NCC and SR models. Thus one may expect significant differences in the properties of NSs obtained for the SR and WR models. This will be explored later in the paper.

The symmetry energy elements $L$ and $K_{\rm sym}$ predominantly determine the value of $K_\tau$ [Eq. (18)] which is required to evaluate the incompressibility of ANM. In Fig. 2 we compare our values of $K_\tau$ with various Skyrme and RMF model predictions in a $K$ vs $K_\tau$ plot [43]. The dashed lines represent the constraints on $K_\tau$ from $-840$ to $-350$ MeV [44–46] and $K$ from 220 to 260 MeV [47] which have been determined using various experimental data on isoscalar giant monopole resonances. All three models NCC, SR, and WR satisfy these bounds of $K$ and $K_\tau$. Note that the models with a larger nuclear incompressibility ($K$) tend to have lower $K_\tau$ values. As can be seen from Fig. 2, several Skryme models but only three RMF models (NLC, DDME1, and DDME2) satisfy the bounds for $K$ and $K_\tau$ simultaneously. The values of $L$ for the nonlinear model NLC with constant coupling is 107.97 MeV [49] and that for the DDME models with density-dependent coupling constants are 51–55 MeV [49]. The value of $L$ for the NLC model is very large compared to the presently accepted range. We have also looked into the values of $K_\tau$ and $K$ for several nonlinear RMF models [50]. Among them a few models (BSR type) have $L$ between 60 and 70 MeV and satisfy the constraints on $K$ and $K_\tau$. These models include both $\sigma$-$\rho$ and $\omega$-$\rho$ cross-couplings.

In Fig. 3 we plot the low-density EOS for PNMs for all three of our models (NCC, SR, and WR). The low-density behavior of energy per neutron for the SR model is in good agreement with the results obtained by microscopic calculations [51,52] as shown by the shaded region. The PNM EOS for the NCC and WR models do not have much overlap with the shaded region. The results for the few selected RMF models are also displayed in the figure. Only the BSP model shows marginal overlap with the shaded region. In Ref. [53] two different families of systematically varied models with $\sigma$-$\rho$ and $\omega$-$\rho$ cross-couplings have been employed to study the low-density behavior of asymmetric nuclear matter. It was found that none of the models with $\sigma$-$\rho$ cross-coupling satisfy the low-density behavior of the PNM as predicted by Hebeler *et al.* [52]. However, this constraint on the PNM EOS at low densities is satisfied by a couple of RMF models with $\omega$-$\rho$ cross-coupling having $L \sim 45-65$ MeV. The EOS with the current parametrization is compared in Fig. 4 with the experimental flow data obtained from the HIC [54] for SNM and PNM EOSs. The latter one is constructed theoretically

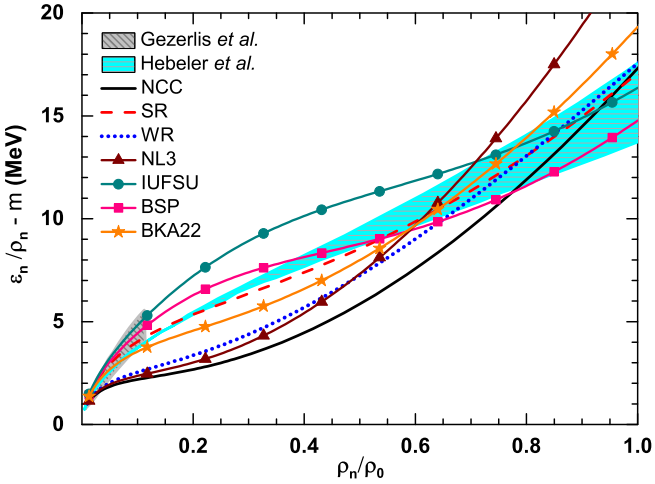


FIG. 3. Energy per neutron as a function of scaled neutron density ($\rho_n/\rho_0$) for three different variants of the effective chiral model as labeled by NCC, SR, and WR obtained in the present work and for a few RMF models NL3, IUFSU, BSP, and BKA22 are compared with microscopic calculations [51,52] as shown by the shaded region.

with two extreme parametrizations, the weakest (Asy soft) and strongest (Asy stiff) of symmetry energy as proposed in [55] and as reported in [54]. The SNM EOS is identical for all three of our models, since the SNM properties are same. It is passing well through the experimental HIC data. In the case of the PNM, the resulting EOSs for NCC and SR models pass through the upper end of HIC-Asy soft and lower end of HIC-Asy stiff, whereas the PNM EOS for the WR model passes through the HIC-Asy soft only. As can be seen from Fig. 4, the influence of cross-couplings in the effective chiral

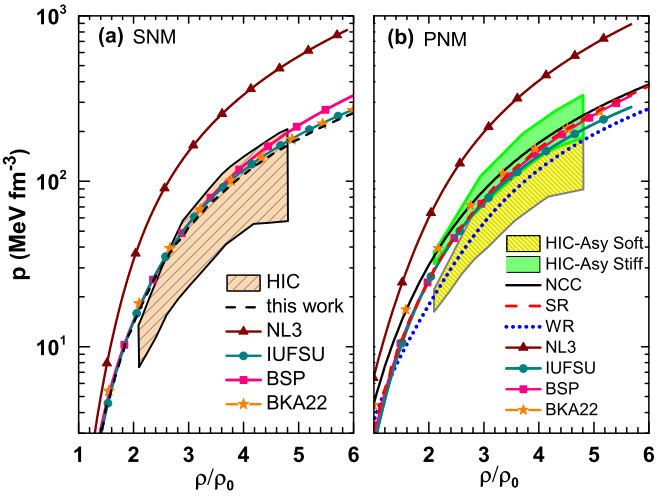


FIG. 4. Pressure as a function of scaled density ($\rho/\rho_0$) for the SNM (left) and the PNM (right). The SNM EOSs for the NCC, SR, and WR models are exactly the same and labeled as "this work." For comparison, the SNM and PNM EOSs for a few RMF models NL3, IUFSU, BSP and BKA22 are displayed. The SNM and PNM EOSs shown by shaded regions are taken from Ref. [54] (see text for details).

model at high density is quite strong in comparison to RMF models with similar type of cross-couplings. The PNM EOS for the WR model is quite softer than BSP and IUFSU at high densities. Similar differences can also be seen in the case of SR and BKA22 models.

We extend our analysis to study the mass-radius relationship for a static NS composed of $\beta$ equilibrated charge neutral matter. The EOS for the core is obtained from the effective chiral model. The effects of crustal EOS at low densities on the mass and radius of the NS are considered in two different ways. We model the crust EOS using the BPS EOS [56] in the density range $\rho \sim 4.8 \times 10^{-9}$ to $2.6 \times 10^{-4}$ fm$^{-3}$. The crust and core are joined using the polytropic form [57] $p(\epsilon) = a_1 + a_2\epsilon^{\gamma}$, where the parameters $a_1$ and $a_2$ are determined in such a way that the EOS for the inner crust for a given $\gamma$ matches with that for the inner edge of the outer crust at one end and with the edge of the core at the other end. The polytropic index $\gamma$ is taken to be equal to 4/3. For $\gamma = 4/3$, the values of radius $R_{1.4}$ corresponding to the canonical mass of the NS for the NL3 [57] and IUFSU [58] RMF models are within ∼2% in comparison to those obtained by treating the inner crust in the Thomas Fermi approach [59]. Alternatively, we estimate the contributions of the crust EOS to the NS radius and mass using the core-crust approximation approach given in [32] referred to hereafter as the ZFH method. This method enables one to estimate total mass and radius of a NS including the crust contributions very accurately for NS masses larger than $1M_{\odot}$. In the ZFH method the radius and mass of the NS are given by

$$R = \frac{R_{\rm core}}{1-(\alpha-1)(R_{\rm core}c^2/2GM-1)}, \tag{19}$$

$$M = M_{\rm crust} + M_{\rm core}, \tag{20}$$

with

$$M_{\rm crust} = \frac{4\pi P_{\rm cc} R_{\rm core}^4}{GM_{\rm core}}\left(1-\frac{2GM_{\rm core}}{R_{\rm core}c^2}\right). \tag{21}$$

In the above equations $\alpha = (\mu_{\rm cc}/\mu_0)^2$, $\mu_{\rm cc}$, and $\mu_0$ are the chemical potential at transition density ($\rho_{\rm cc}$) and at the neutron star surface, respectively. $R_{\rm core}$ and $M_{\rm core}$ are the radius and mass of the NS core. $P_{\rm cc}$ is pressure at transition density. The transition density ($\rho_{\rm cc}$) is mostly in the range $0.4\rho_0$ to $0.6\rho_0$ for $L$ typically ranging from 30 to 120 MeV [60]. In the present work we have taken $\rho_{\rm cc}/\rho_0 = 0.3$, 0.4, and 0.5.

Comparison of the results of the two approaches is given in Table III. The maximum mass of the NS is sensitive to neither the methods used to estimate the crust effects nor the choice of transition density. The WR model, which includes the $\omega$-$\rho$ cross-coupling, does not satisfy the maximum mass constraint as imposed by PSR $J0348+0432\,(M = 2.01 \pm 0.04M_{\odot})$ [61]. This disfavors the WR model. The values of $R_{1.4}$ obtained using the BPS EOS for the outer crust and polytropic EOS for the inner crust are a little too large compared to those for the ZFH method. We find that by including the $\sigma$-$\rho$ coupling (SR) $R_{1.4}$ are smaller compare to the NCC model which does not include any cross-coupling term. The NS radius is sensitive to transition density. Using the strong correlation between transition density ($\rho_{\rm cc}$) and $L$, we found the values of $\rho_{\rm cc}$ to be 0.061 fm$^{-3}$ (∼ $0.4\rho_0$) for NCC and 0.077 fm$^{-3}$ (∼ $0.5\rho_0$)

TABLE III. Maximum mass and radius of a NS composed of $\beta$-equilibrated matter. The total mass and radii following the ZFH method are obtained by using Eqs. (19)–(21). These are compared with the ones calculated from the BPS and polytropic EOSs for the outer and inner crusts, respectively. $\rho_{cc}/\rho_0$ is the scaled transition density. $M_{max}$, $R_{max}$, and $R_{1.4}$ are the NS maximum mass, radius at maximum mass, and the radius at $1.4M_\odot$, respectively.

| $\frac{\rho_{cc}}{\rho_0}$ | Model | BPS+polytropic EOS | | | ZFH method | | |
|---|---|---|---|---|---|---|---|
| | | $M_{max}$ ($M_\odot$) | $R_{max}$ (km) | $R_{1.4}$ (km) | $M_{max}$ ($M_\odot$) | $R_{max}$ (km) | $R_{1.4}$ (km) |
| 0.3 | NCC | 1.97 | 11.55 | 13.31 | 1.97 | 11.48 | 13.12 |
| | SR | 1.97 | 11.24 | 12.75 | 1.97 | 11.20 | 12.71 |
| | WR | 1.84 | 10.74 | 12.22 | 1.84 | 10.67 | 12.03 |
| 0.4 | NCC | 1.97 | 11.64 | 13.57 | 1.97 | 11.48 | 13.12 |
| | SR | 1.97 | 11.28 | 12.87 | 1.97 | 11.21 | 12.72 |
| | WR | 1.84 | 10.83 | 12.41 | 1.84 | 10.67 | 12.03 |
| 0.5 | NCC | 1.97 | 11.77 | 13.90 | 1.97 | 11.50 | 13.13 |
| | SR | 1.97 | 11.35 | 13.04 | 1.97 | 11.24 | 12.72 |
| | WR | 1.84 | 10.92 | 12.62 | 1.84 | 10.67 | 12.03 |

for SR and WR models, respectively [59]. The mass-radius relationships for the NS obtained by all of our models using the respective values of the transition densities are plotted in Fig. 5. The dashed lines are obtained using the ZFH method in which the effects of the crust EOS were approximated and the solid lines are obtained using BPS and the polytropic EOSs for the outer and inner crusts, respectively. It is found that the value of $R_{1.4}$ is decreased by $\sim$0.5 km in the SR model compared to the NCC model. The $R_{1.4}$ of SR is consistent with $11.9 \pm 1.22$ km (90% confidence) obtained by constraining symmetry energy at saturation density from various experimental information and theories [34]. The NS maximum masses $M_{max} = 2.79M_\odot$, $1.94M_\odot$, $2.02M_\odot$, and $2.04M_\odot$ and the radii $R_{1.4} =$ 14.66, 12.49, 12.64, 13.28 km

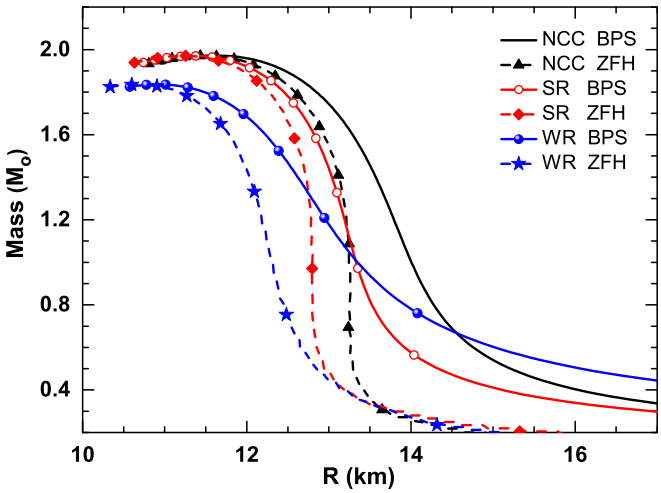


FIG. 5. Mass-radius relationships for the NCC, SR, and WR models. The effects of the crustal EOSs are incorporated by using explicitly the BPS and polytropic EOSs (solid lines) at low densities and alternatively using the ZFH method (dashed lines).

for the selected RMF models NL3, IUFSU, BSP, and BKA22, respectively. The RMF models such as IUFSU and BSP with the $\omega$-$\rho$ cross-coupling included readily yield $M_{max} \sim 2M_\odot$, since the softening of the EOS due to the inclusion of this cross-coupling is not as strong as in the case of the effective chiral model.

Results obtained for the SR model can be summarized in the following way. It yields symmetry energy $J_0 = 32.5$ MeV, symmetry energy slope parameter $L = 65$ MeV, nuclear incompressibility $K = 247$ MeV, and the asymmetry term of nuclear incompressibility $K_\tau = -368$ MeV at saturation density $\rho_0 = 0.153$ fm$^{-3}$. It also yields symmetry energy $J_1 =$ 24.49 MeV at density 0.1 fm$^{-3}$, NS maximum mass $1.97M_\odot$, and radius $R_{1.4} = 12.72$ km. All these values are within the presently accepted range. The SR model also satisfies all the discussed constraints from microscopic calculations for low-density PNM EOS, density dependence of symmetry energy, HIC data for SNM EOS, and HIC-Asy stiff data for PNM EOS.

The contributions of the exotic degrees of freedom, such as hyperons and kaons, to the properties of NSs are not considered in the present work. In general, the presence of strange particles softens the EOS and reduces the NS maximum mass. In particular, the inclusion of hyperons in the effective chiral model (i.e., NCC type) tends to reduce the NS maximum mass by $\sim 0.3M_\odot$ [30]. The influence of hyperons on the NS properties, however, are very sensitive to the choice of the meson-hyperon couplings. It has been shown that a sizable fraction of hyperons may exist in the NS with a mass of $2M_\odot$, provided a strong, repulsive, hyperon-hyperon interaction is introduced through strange $\phi$ mesons [62–64].

## IV. CONCLUSION

We have extended the effective chiral model by including the contributions from $\sigma$-$\rho$ and $\omega$-$\rho$ cross-couplings. The inclusion of cross-couplings involving the $\rho$ meson has helped to improve the overall behavior of the density dependence of the symmetry energy.

We have discussed three different variants of the effective chiral model in this paper. The models include no cross-coupling (NCC), $\sigma$-$\rho$ cross-coupling (SR), and $\omega$-$\rho$ cross-coupling (WR). The NCC model yields the value of symmetry energy slope parameter ($L = 87$ MeV) which is a little too large and symmetry energy at crossing density 0.1 fm$^{-3}$ ($J_1 =$ 22.3 MeV) which is low compared to presently estimated values. The low-density behavior of PNM EOS for both NCC and WR models does not match well with the range of values proposed by microscopic calculations [51,52]. The WR model gives the NS maximum mass to be $1.86M_\odot$ which is much less than the mass observed for the PSR $J0348 + 0432$ ($M = 2.01 \pm 0.04M_\odot$) [61].

For the SR model, the overall behavior of the density dependence of the symmetry energy agrees better with IAS, HIC Sn+Sn, and ASY-EOS data than those for the NCC and WR models. The symmetry energy at the saturation density and at the crossing density ($\rho_1 = 0.1$ fm$^{-3}$) are in harmony with the available empirical data. The value of the symmetry energy slope and the curvature parameters are in accordance with

those deduced from the diverse set of experimental data for the finite nuclei. The pure neutron matter EOS at subsaturation densities passes well through the range of values suggested by the microscopic models [51,52]. The NS maximum mass is $1.97M_{\odot}$ which is consistent with the observational constraint. The value of $R_{1.4}$ is within the empirical bounds. The SR model satisfies all the discussed constraints, which suggests that the inclusion of $\sigma$-$\rho$ cross-coupling in the effective chiral model is indispensable. We have also compared our results with a few selected RMF models. In general, it is found that the effects of various cross-couplings within the RMF models are weaker than those in the effective chiral model. These effects are more prominent for the models with the $\omega$-$\rho$ cross-coupling.

## ACKNOWLEDGMENTS

T.M. thanks SINP for the hospitality provided during his visit for this work and also thanks Chiranjib Mondal and Naosad Alam for useful comments. T.M. and T.K.J. thank DAE-BRNS for its support (2013/37P/5/BRNS).

[1] L. Trippa, G. Colo, and E. Vigezzi, Phys. Rev. C **77**, 061304 (2008).
[2] P. Möller, W. D. Myers, H. Sagawa, and S. Yoshida, Phys. Rev. Lett. **108**, 052501 (2012).
[3] M. B. Tsang *et al.*, Phys. Rev. C **86**, 015803 (2012).
[4] X. Roca-Maza, M. Brenna, G. Colò, M. Centelles, X. Viñas, B. K. Agrawal, N. Paar, D. Vretenar, and J. Piekarewicz, Phys. Rev. C **88**, 024316 (2013).
[5] X. Viñax, M. Centelles, X. Roca-Maza, and M. Warda, Eur. Phys. J. A **50**, 27 (2014).
[6] X. Roca-Maza, X. Viñax, M. Centelles, B. K. Agrawal, G. Colo', N. Paar, J. Piekarewicz, and D. Vretenar, Phys. Rev. C **92**, 064304 (2015).
[7] C. Mondal, B. K. Agrawal, J. N. De, and S. K. Samaddar, Phys. Rev. C **93**, 044328 (2016).
[8] B. G. Todd-Rutel and J. Piekarewicz, Phys. Rev. Lett. **95**, 122501 (2005).
[9] B. K. Agrawal, Phys. Rev. C **81**, 034323 (2010).
[10] B. K. Agrawal, A. Sulaksono, and P. G. Reinhard, Nucl. Phys. A **882**, 1 (2012).
[11] M. Gell-Mann and M. Levy, Nuovo Cimento **16**, 705 (1960).
[12] T. D. Lee and G. C. Wick, Phys. Rev. D **9**, 2291 (1974).
[13] T. D. Lee and M. Margulies, Phys. Rev. D **11**, 1591 (1975); **12**, 4008(E) (1975).
[14] A. W. Thomas, P. A. M. Guichon, D. B. Leinweber, and R. D. Young, Prog. Theor. Phys. Suppl. **156**, 124 (2004).
[15] R. J. Furnstahl and B. D. Serot, Phys. Lett. B **316**, 12 (1993).
[16] E. K. Heide, S. Rudaz, and P. J. Ellis, Nucl. Phys. A **571**, 713 (1994).
[17] I. Mishustin, J. Bondorf, and M. Rho, Nucl. Phys. A **555**, 215 (1993).
[18] P. Papazoglou, J. Schaffner, S. Schramm, D. Zschiesche, H. Stöcker, and W. Greiner, Phys. Rev. C **55**, 1499 (1997).
[19] P. Papazoglou, S. Schramm, J. Schaffner-Bielich, H. Stöcker, and W. Greiner, Phys. Rev. C **57**, 2576 (1998).
[20] S. Schramm, Phys. Rev. C **66**, 064310 (2002).
[21] K. Tsubakihara and A. Ohnishi, Prog. Theor. Phys. **117**, 903 (2007).
[22] K. Tsubakihara, H. Maekawa, and A. Ohnishi, Eur. Phys. J. A **33**, 295 (2007).
[23] K. Tsubakihara, H. Maekawa, H. Matsumiya, and A. Ohnishi, Phys. Rev. C **81**, 065206 (2010).
[24] J. Boguta, Phys. Lett. B **128**, 19 (1983).
[25] P. K. Sahu, R. Basu, and B. Datta, Astrophys. J. **416**, 267 (1993).
[26] P. K. Sahu and A. Ohnishi, Prog. Theor. Phys. **104**, 1163 (2000).
[27] P. K. Sahu, T. K. Jha, K. C. Panda, and S. K. Patra, Nucl. Phys. A **733**, 169 (2004).
[28] T. K. Jha and H. Mishra, Phys. Rev. C **78**, 065802 (2008).
[29] D. Logoteta, I. Vidaña, I. Bombaci, and A. Kievsky, Phys. Rev. C **91**, 064001 (2015).
[30] T. K. Jha, P. K. Raina, P. K. Panda, and S. K. Patra, Phys. Rev. C **74**, 055803 (2006); **75**, 029903(E) (2007).
[31] X. Roca-Maza, M. Brenna, B. K. Agrawal, P. F. Bortignon, G. Colò, L.-G. Cao, N. Paar, and D. Vretenar, Phys. Rev. C **87**, 034301 (2013).
[32] J. L. Zdunik, M. Fortin, and P. Haensel, Astron. Astrophys. **599**, A119 (2017).
[33] J. Dong, W. Zuo, and J. Gu, Phys. Rev. C **91**, 034315 (2015).
[34] J. M. Lattimer and Y. Lim, Astrophys. J. **771**, 51 (2013).
[35] L.-W. Chen, B.-J. Cai, C. M. Ko, B.-A. Li, C. Shen, and J. Xu, Phys. Rev. C **80**, 014322 (2009).
[36] P. K. Sahu, K. Tsubakihara, and A. Ohnishi, Phys. Rev. C **81**, 014002 (2010).
[37] B.-A. Li and X. Han, Phys. Lett. B **727**, 276 (2013).
[38] G. A. Lalazissis, J. Konig, and P. Ring, Phys. Rev. C **55**, 540 (1997).
[39] F. J. Fattoyev, C. J. Horowitz, J. Piekarewicz, and G. Shen, Phys. Rev. C **82**, 055803 (2010).
[40] M. B. Tsang, Y. Zhang, P. Danielewicz, M. Famiano, Z. Li, W. G. Lynch, and A. W. Steiner, Phys. Rev. Lett. **102**, 122701 (2009); Int. J. Mod. Phys. E **19**, 1631 (2010).
[41] P. Danielewicz and J. Lee, Nucl. Phys. A **922**, 1 (2014).
[42] P. Russotto *et al.*, Phys. Rev. C **94**, 034608 (2016).
[43] H. Sagawa, S. Yoshida, G.-M. Zeng, J.-Z. Gu, and X.-Z. Zhang, Phys. Rev. C **76**, 034327 (2007); **77**, 049902(E) (2008).
[44] J. R. Stone, N. J. Stone, and S. A. Moszkowski, Phys. Rev. C **89**, 044316 (2014).
[45] J. M. Pearson, N. Chamel, and S. Goriely, Phys. Rev. C **82**, 037301 (2010).
[46] T. Li *et al.*, Phys. Rev. C **81**, 034309 (2010).
[47] S. Shlomo, V. M. Kolomietz, and G. Colò, Eur. Phys. J. A **30**, 23 (2006).
[48] G. Colo, U. Garg, and H. Sagawa, Eur. Phys. J. A **50**, 26 (2014).
[49] M. Dutra, O. Lourenço, S. S. Avancini, B. V. Carlson, A. Delfino, D. P. Menezes, C. Providência, S. Typel, and J. R. Stone, Phys. Rev. C **90**, 055203 (2014).
[50] N. Alam, B. K. Agrawal, M. Fortin, H. Pais, C. Providência, A. R. Raduta, and A. Sulaksono, Phys. Rev. C **94**, 052801 (2016).
[51] A. Gezerlis and J. Carlson, Phys. Rev. C **81**, 025803 (2010).
[52] K. Hebeler, J. M. Lattimer, C. J. Pethick, and A. Schwenk, Astrophys. J. **773**, 11 (2013).
[53] N. Alam, H. Pais, C. Providência, and B. K. Agrawal, Phys. Rev. C **95**, 055808 (2017).

[54] P. Danielewicz, R. Lacey, and W. G. Lynch, Science **298**, 1592 (2002).
[55] M. Prakash, T. L. Ainsworth, and J. M. Lattimer, Phys. Rev. Lett. **61**, 2518 (1988).
[56] G. Baym, C. Pethick, and P. Sutherland, Astrophys. J. **170**, 299 (1971).
[57] J. Carriere, C. J. Horowitz, and J. Piekarewicz, Astrophys. J. **593**, 463 (2003).
[58] J. Piekarewicz, F. J. Fattoyev, and C. J. Horowitz, Phys. Rev. C **90**, 015803 (2014).
[59] F. Grill, H. Pais, C. Providência, I. Vidaña, and S. S. Avancini, Phys. Rev. C **90**, 045803 (2014).
[60] C. Ducoin, J. Margueron, C. Providencia, and I. Vidana, Phys. Rev. C **83**, 045810 (2011).
[61] J. Antoniadis *et al.*, Science **340**, 6131 (2013).
[62] S. Weissenborn, D. Chatterjee, and J. Schaffner-Bielich, Nucl. Phys. A **881**, 62 (2012).
[63] A. Sulaksono and B. K. Agrawal, Nucl. Phys. A **895**, 44 (2012).
[64] D. Bizarro, A. Rabhi, and C. Providência, arXiv:1502.04952.